

SCALING OF MIXED CONVECTION IN AIRCRAFT CABINS

A. Westhoff, J. Bosbach and C. Wagner

German Aerospace Center - Institute of Aerodynamics and Flow Technology, Bunsenstrasse 10,
37073 Göttingen, Germany

Keywords: *Mixed Convection, Scaling, POD, Indoor Climatisation, Particle Image Velocimetry*

Abstract

For the present study of turbulent mixed convection a generic convection cell has been developed. It was designed to work with air as working fluid under high pressure as well as ambient pressure conditions. Based on Particle Image Velocimetry (PIV) and temperature measurements a concept which allows to scale the spatial dimension at turbulent mixed convection by increasing the fluid pressure and adjusting the inflow velocity has been studied. Further analyse the spatial structure of the kinetic energy distribution in mixed convection Proper Orthogonal Decomposition (POD) calculations of the velocity fields have been performed. Results of these investigations are presented.

1 Introduction

Mixed convection is an important type of flow which is characterised by the interaction between forced and free convection occurring as a result of buoyancy-induced motion. It is present in many technical applications like e.g. heat exchangers [14], air conditioning of passenger departments [13] or indoor climatisation [3]. Moreover, mixed convection is a typical phenomenon in geology and meteorology and occurs often at large scales. Hence, a direct experimental investigation is difficult or sometimes even impossible.

A measurement method which allows to study large scale mixed convection at reduced model size by keeping the characteristic non-dimensional parameters constant, i.e. Grashof

number Gr , Reynolds number, Re , and Prandtl number, Pr constant, is highly desirable. In the past scaling of mixed convection was accomplished by choosing a different working fluid with a lower kinematic viscosity. For example Linden [2] developed a scaling concept for investigations of indoor climatisation by scaling the Re and Peclet number Pe , using water as working fluid and brine to create a density gradient. With this approach he was able to scale the model size by a factor of 1:20 - 1:100. The drawback of his approach is the use of a fluid with a different Pr and therefore a change of fluid properties. Therefore, the approach of the scaling concept presented here is to reduce the spatial dimensions of such configurations to scales which are experimentally accessible by increasing the fluid pressure, adjusting the inflow velocity and thus keeping Gr , Re and Pr constant.

Before getting back to turbulent mixed convection, we will consider some related set-ups and measurement techniques applied to purely thermal convection in enclosures heated from below and cooled from above. A lot of attention has been drawn to studies of thermal convection using highly pressurised gases to achieve high Rayleigh numbers. Fleischer and Goldstein used e.g. highly pressurised nitrogen to study Rayleigh-Bénard convection at high Ra in a cylindrical horizontal container [4]. They investigated the Nusselt-Rayleigh heat transfer relationship for $1 \cdot 10^9 < Ra < 1.7 \cdot 10^{12}$ and also recorded Schlieren video images. The maximum Ra has been reached at a pressure of 80 bar for a characteristic length of $L = 0.45$ m. For sev-

eral other studies reported in the literature different pressurised gases have been used. For example Niemela *et al.* [5] used cryogenic helium to study Nusselt-Rayleigh heat transfer relationship at very high Ra up to 10^{17} . An other thermal convection experiment has been performed by Xia *et al.* [12]. They studied large-scale circulation for different Ra using water as working fluid, in a rectangular container with an isothermal bottom and ceiling by means of PIV.

A mixed convection experiment comparable to our experimental set-up has been used by Linden *et al.* [1,2]. They explored the heat transfer and flow structures in what they called natural ventilation with one or more heat sources to induce buoyancy forces and several in- and outlet locations on a down-scaled cavity with water as working fluid. The aim of their studies was to extend the possibilities for living and working under inclement or inhospitable conditions. Another study with a comparable set-up is the Laser Doppler Anemometry (LDA) of mixed convection in a rectangular tube with isothermal bottom and ceiling filled with nitrogen [6,7]. In contrast to our experiment, they studied mixed convection for lower Rayleigh numbers in the range $2472 < Ra < 8300$, as well as $15 < Re < 150$ and $0.5 \lesssim Ar \lesssim 2$. Ar is the Archimedes number, which is defined by the ratio of buoyancy and inertia forces. However, to our knowledge, PIV of turbulent mixed convection at high fluid pressure, has not been performed so far.

At the German Aerospace Centre in Göttingen a modularly designed convection cell was developed to study mixed convection for $600 < Re < 3 \cdot 10^6$, $5 \cdot 10^5 < Gr < 5 \cdot 10^{10}$. In order to cover these Re and Gr regimes the cell can be operated in a pressure range of $1 < p < 100$ bar. The aim is to apply PIV at high pressure in order to study the effect of high pressure on the dynamics of coherent structures and heat transfer considering the scaling concept which will make possible to measure aircraft cabin air flow using downscaled models in the future.

2 Scaling concept

Mixed convection in a given geometry is characterised by the non-dimensional parameters

$$Gr = \frac{g\alpha\Delta TH^3}{\nu^2}, \quad (1)$$

$$Re = \frac{UL}{\nu} \quad (2)$$

and

$$Pr = \frac{\nu}{\kappa}, \quad (3)$$

where g denotes the gravitational acceleration, H the height of the cell, $\alpha = -1/\rho(\partial\rho/\partial T)$ the thermal expansion coefficient, ν the kinematic viscosity, κ the thermal diffusivity, v_{in} the inlet velocity, ρ the density and L the characteristic length scale of the system. An additional parameter to characterise mixed convection is the Archimedes number

$$Ar = \frac{\sqrt{Gr}}{Re}, \quad (4)$$

which is the ratio of buoyancy and inertia forces. For the considered case the characteristic length in eq. 2 is equal to the height of the cell.

Often one would like to study the flow with the same nondimensional parameters but in a geometry whose size \hat{H} is by a factor s smaller than its original size, i.e. $\hat{H} = s_H \cdot H$. Scaling theory tells us how one has to adjust velocity, viscosity, thermal diffusivity and the thermal expansion coefficient in order to accomplish this task. Assuming that the thermal expansion coefficient is independent of pressure for our working fluid air one can readily verify that the scaling coefficients for the mentioned quantities are related to s by the equations

$$Gr = \frac{g\alpha\Delta T(s_H H)^3}{s_\nu^2 \nu^2}, \quad (5)$$

$$Re = \frac{s_U U s_L L}{s_\nu \nu} \quad (6)$$

and

$$Pr = \frac{s_\nu \nu}{s_\kappa \kappa}. \quad (7)$$

The corresponding scaling factors are denoted as s_i . Under the constraint of geometrical similarity, i.e. $s_L = s_H$, we obtain the two equations

$$s_v = (s_H)^{\frac{3}{2}} \text{ and } s_{v_{in}} = (s_H)^{\frac{1}{2}}. \quad (8)$$

Scaling of the system by a factor s_H for the height of the container yields the scaling factors for kinematic viscosity s_v and the inflow velocity $s_{v_{in}}$. Since μ , the dynamic viscosity, is unaffected by the pressure for $1 < p < 30$ bar, the kinematic viscosity can be controlled linearly via the density ρ , which in turn depends on the pressure p . Otherwise for a fluid pressure $p > 30$ bar the kinematic viscosity has to be adjusted with an experimentally defined formula given by Smits and Zagarola [8].

3 Analytical method

The instantaneous velocity fields are analysed using the Proper Orthogonal Decomposition (POD) procedure based on the snapshots method by Sirovich [10,11]. Given is a set of N two dimensional two component instantaneous velocity fields

$$\underline{U}^{(n)}(\underline{x}) = (u_1^{(1)}, \dots, u_l^{(i)}, v_1^{(1)}, \dots, v_l^{(i)}), \quad (9)$$

where $1 \leq n \leq N$ denotes the time index, u_i and v_i the velocity components of the size $l = m \times n$ (m dimension in x-direction and n in y-direction). Hence, a set of $\underline{U}^{(n)} = \underline{U}(\underline{x}, n\tau)$ vector fields with a sampling rate τ is given. Then the correlation matrix \underline{K} reads

$$\underline{K} = \frac{1}{N} \sum \underline{U}^{(n)}(\underline{x}) \cdot \underline{U}^{(n)}(\underline{x}'). \quad (10)$$

Solving the eigenvalue equation

$$\underline{K} \underline{\zeta} = \alpha \underline{\zeta} \quad (11)$$

using Singular Value Decomposition (SVD) provides real positive eigenvalues λ_k and the associated eigenvectors $\underline{\zeta}_k$. The energy eigenvalues λ_k are ordered in a decreasing order and the eigenvectors $\underline{\zeta}_k$ define an orthonormal basis. By the linear transformation

$$\underline{\Phi}_k(\underline{x}) = \sum_{i=1}^N \underline{\zeta}_i \underline{U}^{(i)} \quad (12)$$

a new orthogonal basis is determined. In the following the time averaged spatial kinetic energy distribution $\underline{\Phi}_k$ will be called coherent structure.

4 Experimental Set-up

4.1 High Pressure Wind Tunnel

The measurements were performed in the High Pressure Wind Tunnel Göttingen (HDG), which is a Göttingen-type closed circuit low speed wind tunnel that can be pressurised up to 100 bar. The velocity is adjustable between 3.5 and 35 m/s in the total range of pressure. At a temperature of 300 K with the standard reference length definition of 0.06 m, the Reynolds number can be varied up to $1.2 \cdot 10^7$. The test section has a height of 0.6 m, a width of 0.6 m and a length of 1 m.

The purpose of using of the HDG in our experiments is threefold. First it allows to adjust the fluid pressure, second it provides the inflow for our convection cell, and finally it supplies cooling to the cell ceiling.

4.2 Convection cell

The convection cell is a cuboidal container with a quadratic cross section, an air inlet at the top and an air outlet at the bottom. The cell has a width of 0.1 m, a height of 0.1 m and a length of 0.5 m. In- and outlet are located at the same side of the cell. Both span the whole length of the cell and are equipped with rectangular channels of height 5 mm and length 300 mm for the inlet as well as a height of 3 mm and length of 120 mm for the outlet. The inlet channel is equipped with an additional fence in order to further homogenise the inflow. All side walls are thermally insulated by a layer system with an insulating sheath of 7 mm air between two transparent windows in order to accomplish almost adiabatic boundary conditions while maintaining the optical accessibility of the cell.

The floor of the container is equipped with a heated copper plate and the ceiling with an aluminium heat exchanger. Cooling is realized by cooling fins, which provide thermal coupling between the cooling plate and the air in the wind

tunnel.

Resistance Temperature Detectors (RTDs) are embedded in the cooling and heating plate in order to monitor the temperatures of our cell. Further the in- and outflow temperature are also recorded with RTDs. In addition to the temperature the dynamic pressure at the outlet was measured with a Pitot-tube in combination with a static pressure probe in order to determine the average inflow velocity \hat{v}_{in} .

With this configuration we are able to generate mixed convection under well defined conditions and adjustable fluid pressure. Further informations about the cell set-up can be found in Westhoff et. al. [15,16].

4.3 Particle Image Velocimetry set-up

The 2D-2C Particle Image Velocimetry (PIV) has been applied in order to measure mixed convection in our cell under high pressure conditions. The PIV system consists of a double oscillator quality switched Nd:YAG laser, light sheet optics and a Peltier-cooled charge coupled device (CCD) camera (1376x1040 spatial resolution at 12 bit grayscale), which is placed in front of the convection cell. The light sheet is injected into the cell from the opposite side of the air inlet. According to the optical set-up only the velocity parallel to the light sheet plane were detected (2C-2D PIV). As seeding solid particles of Matroxid (Al_2O_3) with diameters of about μm were used. They were injected into the flow by a fluidised-bed seeding generator (a detailed description is given in Willert and Jarius [9]). Finally, the PIV measurement plane is located at 50 % in longitudinal direction.

5 Results

Eigenvalues λ_i , time coefficients $\underline{\zeta}_i$ and coherent structures Φ_i are computed as explained before. These POD results will be compared with the structure of the time averaged velocity fields and the time series of the measured temperature at the outlet. First we compare the structure of the time averaged velocity map with the coherent

Table 1 Measurement conditions for mixed convection at 5.1 bar.

Ar	Re	Gr	ΔT [K]	\tilde{v}_{in} [m/s]
0.89	$1.1 \cdot 10^4$	$9.5 \cdot 10^7$	30.1	0.35
1.24	$7.7 \cdot 10^3$	$9.2 \cdot 10^7$	29.9	0.25
1.60	$6.0 \cdot 10^3$	$9.2 \cdot 10^7$	29.9	0.19

structures of the most relevant modes for 3 different Ar and fluid pressure of 5.1 bar. Details of the measurement conditions are given in Table 1, where ΔT denotes the temperature difference between the cooling and heating device and \tilde{v}_{in} the inflow velocity averaged over the inlet height. It should be noted, that we restrict the discussion to the structure of the POD modes and the time averaged velocity fields. Hence, coherent structures are normalised by the maximal kinetic energy value and the time averaged velocity maps by the maximal velocity. In the structure maps zero is coded dark blue, the intermediate range green and one is coloured red. For the sake of visibility in the figures only every second vector is plotted in each direction. The second part is devoted to the comparison between the powerspectrum of the outlet temperature time series and the powerspectrum of the time coefficient $\underline{\zeta}_i$.

5.1 Coherent Structures

5.1.1 Mixed convection for $Ar = 0.89$

In the regime of $Ar < 1$ the flow is mainly dominated by the inertia forces induced by the forced convection. A jet of incoming air enters the cell through in inlet at the top of the right side. It follows the ceiling, detaches and descends at the left sidewall, detaches again, flows parallel to the bottom plate and splits in two parts. Then one part follows the right sidewall towards the inlet and the other one leaves the cell through the outlet at the lower right side. The result is a nearly 2D mean wind rotating in opposite clockwise direction with the core located in the centre of the measurement plane as reflected in the time aver-

aged velocity field shown in Figure 2a and the instantaneous velocity fields (not shown here). Figure 2b reveals the coherent structure of the first mode and is nearly congruent with the structure of the time averaged velocity field.

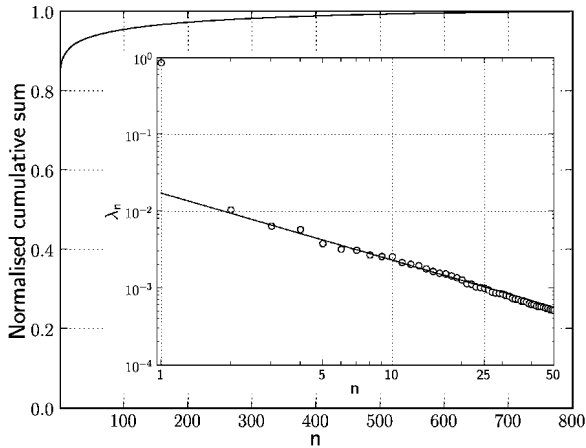


Fig. 1 The convergence of the cumulative sum of the energy eigenvalue and the normalised eigenvalues as function of the mode number n for $Ar = 0.89$.

From this it can be already concluded that in terms of a best approximation the first mode reflects nearly the complete structure of the time averaged velocity field. This can be made even more clear if the energy eigenvalues shown in Figure 1 are considered. The inset in Figure 1 depicts the normalised eigenvalues as function of the mode number n for the 50 first modes. Both axes are scaled logarithmically and the non-relevant eigenvalues are marked by the regression line, which in the literature is called noise level. It can be clearly detected that just the first mode (represents 86 % of the total energy) is above this noise level. Already the second mode contains merely about 1.1 % of the total energy and can be related to the non-relevant eigenvalues. Additionally, the convergence of the normalised cumulative sum of the eigenvalues is plotted in Figure 1. The figure reveals that only the sum of the 6 first modes already represents 90 % of the total energy. Both, coherent structure and eigenvalues show that the flow in the measurement plane is dominated by

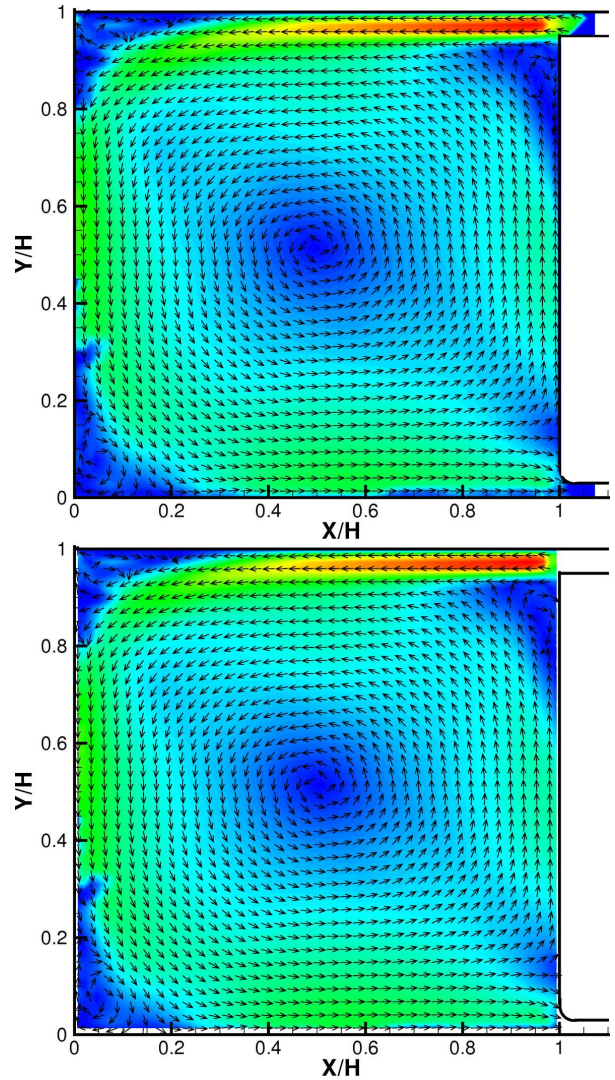


Fig. 2 Coherent and flow structures for $Ar = 0.89$. (a) Top: Time averaged velocity field. (b) Bottom: Coherent structure of the first mode. The magnitude is normalised. Zero is coded dark blue, the intermediate range green and one is coloured red.

forced convection and the influence of the free convection is nearly negligible.

5.1.2 Mixed convection for $Ar = 1.24$

For the case $Ar = 1.24$ the flow is related to the regime of mixed convection. Figure 4 reveals the structure of the time averaged velocity field in the measurement plane. It is observed that the flow is still dominated by nearly the same role structure as that obtained for $Ar = 0.89$. But by increasing

the proportion of the buoyancy-induced motion the centre of the role structure is shifted to the left and thus a break in the symmetry can be found.

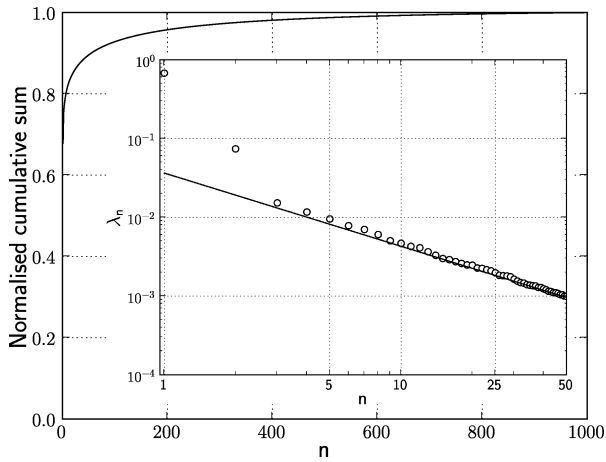


Fig. 3 The convergence of the cumulative sum of the energy eigenvalue and the normalised eigenvalues as function of the mode number n for $Ar = 1.24$.

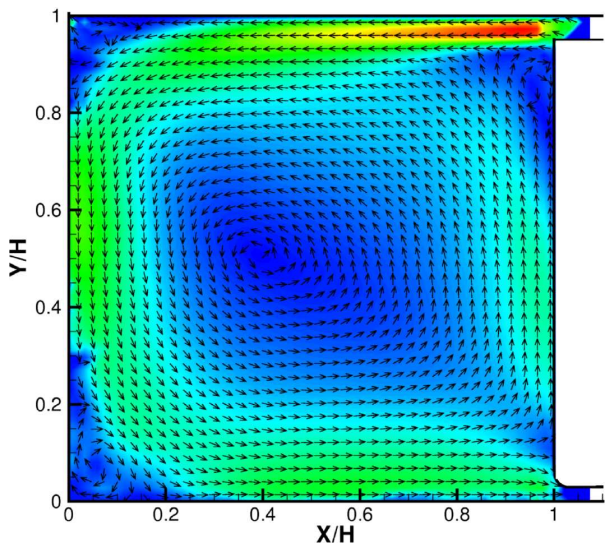


Fig. 4 PIV results for time averaged velocity vector field for $Ar = 1.24$. The magnitude is normalised. Zero is coded dark blue, the intermediate range green and one is coloured red.

Analysing the coherent structures of the first two modes (Figure 5) it is found that the structure of the first mode (Figure 5a), which represent 67 %

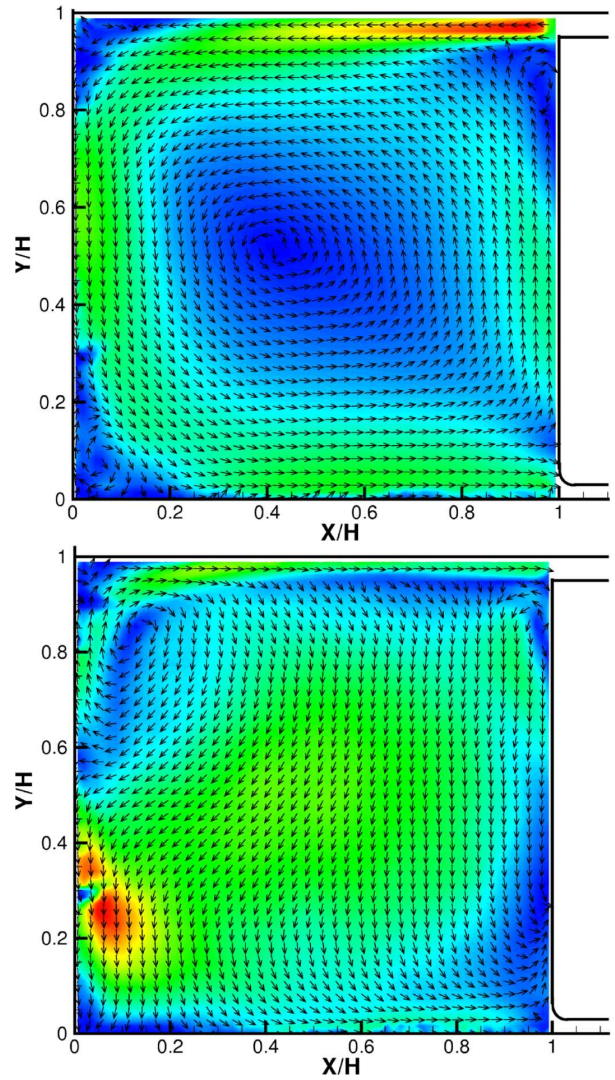


Fig. 5 Coherent structures obtained by POD for $Ar = 1.24$. Top: (a) First mode. Bottom: (b) Second mode. The magnitude is normalised. Zero is coded dark blue, the intermediate range green and one is coloured red.

of the total energy, is nearly concurrent with the time averaged velocity field. In addition to the first mode further modes are becoming relevant as shown in the inset of Figure 4. The figure presents the normalised eigenvalues λ_n as function of the mode number n of the 50 first modes (both axes are scaled logarithmically). It is reflected that the eigenvalue 1 to 8 are above the noise level. Particularly the two first eigenvalues are exceeding the noise level.

The structure of the second mode is depicted

in figure 5b. It is mainly oriented vertical and most of the energy is located at the center and lower left region. This structure represent the buoyancy induced motion of the rising and descending flow. Additionally, it seems that the flow becomes more complex since: (i) the cumulative sum of the 100 first eigenvalues equals 90 % of the total energy and (ii) a lower convergence of the normalised cumulative sum of the eigenvalues (Figure 3) is obtained.

5.1.3 Mixed convection for $Ar = 1.60$

Finally, the structures for $Ar = 1.6$ are discussed. For this Ar it is still the regime of mixed convection whereas the buoyancy-induced motion is becoming dominant. Figure 7 shows the time averaged velocity map. The predominantly symmetric role structure obtained for lower Ar is totally broken. Instead a role structure with one centre located near the centre of the measurement plane, a bimodal structure with one centre in the lower centre region and the other one in the upper left region, has developed.

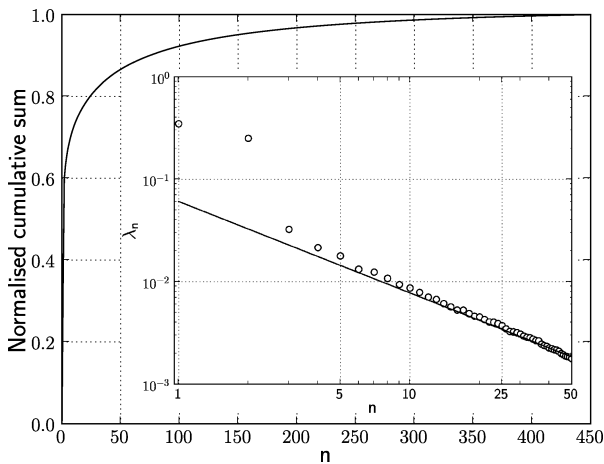


Fig. 6 The convergence of the cumulative sum of the energy eigenvalue and the normalised eigenvalues as function of the mode number n for $Ar = 1.60$.

The POD provides several relevant eigenvalues which exceed the noise level (Figure 6). In addition, the energy of the first mode decreases to 35 % and the second increases to 24 % of the total

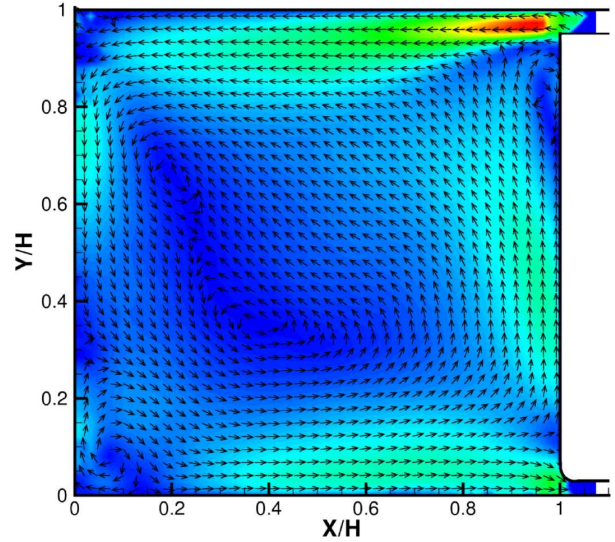


Fig. 7 PIV results for time averaged velocity vector field for $Ar = 1.60$. The magnitude is normalised. Zero is coded dark blue, the intermediate range green and one is coloured red.

energy. Further considering the coherent structure of the first mode (Figure 8a) similarities with the time averaged velocity field can be found. But instead of the structure given in the time averaged velocity map (Figure 7), for the coherent structure of the first mode a role structure with one centre located near the centre of the measurement plane is detected. This structure can be related to the inertia-induced motion, which despite of the structure of the second mode (Figure 8b) can be related to the buoyancy-induced motion. The structure is primarily vertical oriented and the main kinetic energy of this mode is located at the centre of the left side. In addition to the two first modes further modes with energy eigenvalues representing more than 5 % of the total energy are observed. It seems that this modes represent the oscillation of the air jet at the inlet (Figure 9). Considering the instantaneous velocity maps it can be concluded that the wall jet at the ceiling starts to oscillate strongly. Due to this oscillation the jet detaches at different ceiling positions, sometimes already shortly after entering the cell. For this Ar the mean wind depends strongly on the dynamics of the incoming wall jet, that in turn is influenced by the falling

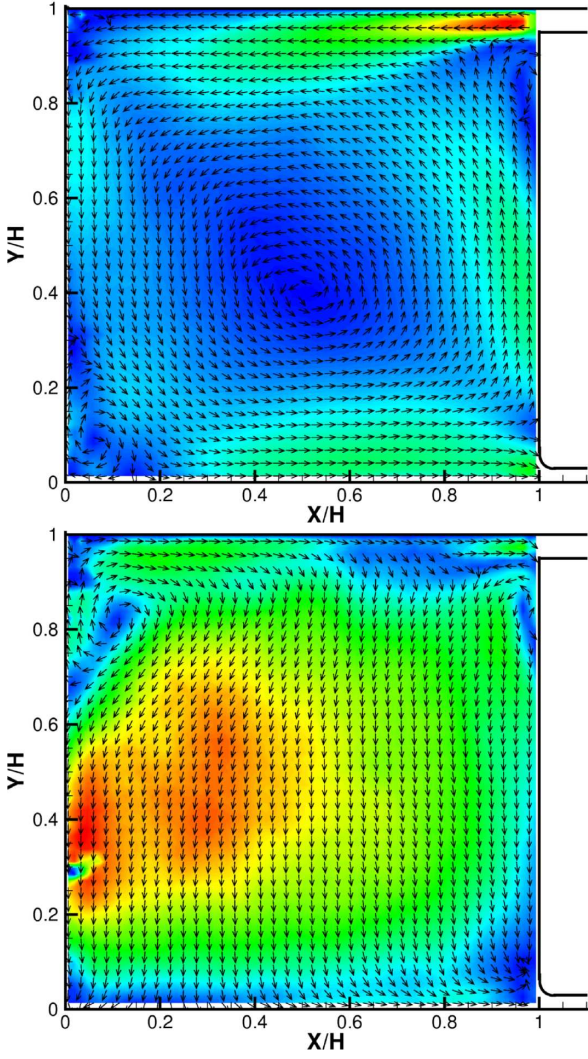


Fig. 8 Coherent structures obtained for $Ar = 1.60$. Top: (a) First mode. Bottom: (b) Second mode. The magnitude is normalised. Zero is coded dark blue, the intermediate range green and one is coloured red.

plumes at the ceiling.

Therefore it can be concluded that for the case of $Ar = 1.6$ a significant increase of eigenvalues which exceed the noise level can be identified. The eigenvalue of the first mode representing the inertia-induced motion decreases strongly and the eigenvalue of the second mode representing the buoyancy-induced motion increases. Due to the larger buoyancy force the role structure is broken and a bimodal structure is formed.

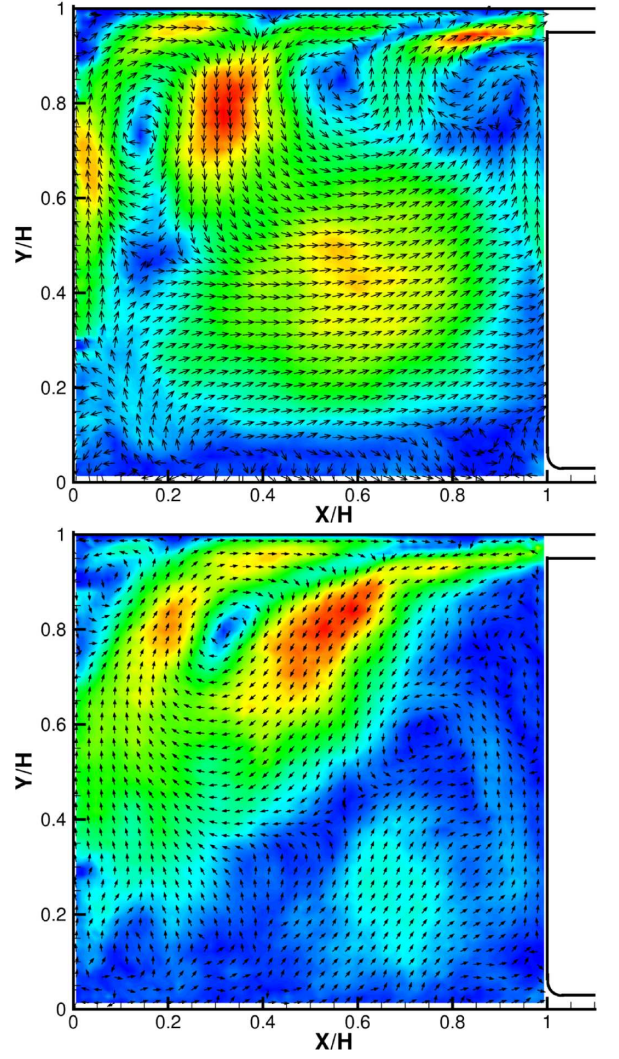


Fig. 9 Coherent structures obtained for $Ar = 1.60$. Top: (a) Third mode. Bottom: (b) Fourth mode. The magnitude is normalised. Zero is coded dark blue, the intermediate range green and one is coloured red.

5.2 Dynamics of the coherent structures

In the following section the discussed dynamics of the coherent structures for the cases $Ar = 1.24$ and $Ar = 1.6$ will be correlated with the outlet temperature time series $\tilde{T}_{out} = T_{out} - T_{in}$ (for both cases the standard derivation of T_{in} is 0.02 K). Examining \tilde{T}_{out} for $Ar = 1.24$ a periodic oscillation in the time signal is observed. The mean level of this oscillation is about 304.61 K, the amplitude about 0.11 K and the frequency $f = 0.008$ Hz. This low frequency oscillation can be also

identified in the powerspectra of the time coefficient $P(\zeta_i(t))$ of the first three modes (Figure 10).

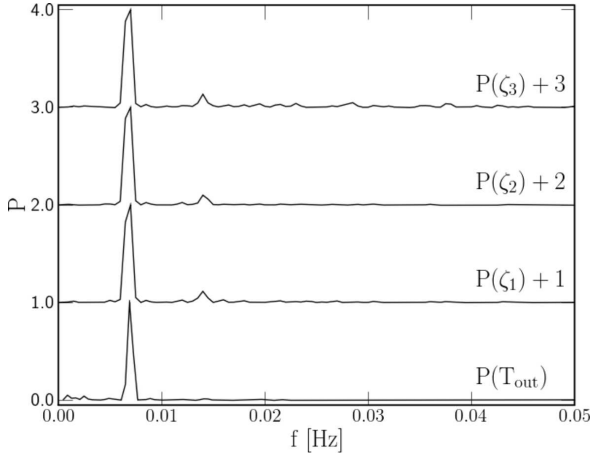


Fig. 10 Normalised powerspectrum P of the outlet temperature time series and the powerspectrum of ζ_i for the first three modes at $Ar = 1.24$.

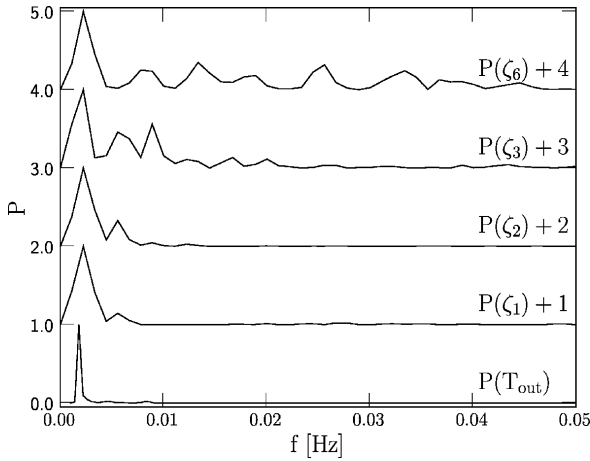


Fig. 11 Normalised powerspectrum P of the outlet temperature time series and the powerspectrum of ζ_i for the first three and the sixth modes at $Ar = 1.6$.

Moreover a phase relation between $P(\zeta_i(t))$ for the first three modes has been found. Analogously to the case $Ar = 1.24$ a low frequency oscillation of \tilde{T}_{out} with $f \approx 0.002$ Hz for the first three modes of $Ar = 1.6$ is observed (fig. 11). Unlike for $Ar = 1.24$ an additional mode $P(\zeta_6(t))$ with the same frequency occurs. Just as for the

case $Ar = 1.24$ and for $Ar = 1.6$ between mode $i = 1, 2, 3, 6$ a fix phase relation exists.

This results yield the assumption that in the measurement plane a recurrent phase related flow condition exists. As a consequence temperature oscillations at the cell outlet have been found. Additionally it can be assumed that in this Ar -regime the oscillation is caused by superposition of two different role structures. One is induced by forced convection which can be identified in the time averaged velocity maps presented (Fig. 2a, 4). Additionally role structures are formed in longitudinal direction induced by thermal convection. Hot air rises at the front and back plate of the cell and in the middle region in longitudinal direction cool air is descending. Depending on the given aspect ratio two oppositionally rotating convection roles are developing. These role structures formed by thermal convection have been also found applying stereo PIV. Due to the limited space these results are not shown here and will be published elsewhere.

6 Conclusion

Mixed convection using pressurised air as working fluid has been experimentally investigated in a rectangular container. Using POD, coherent structures $\Phi_i(x)$ with the related time coefficient $\zeta_i(t)$ and the eigenvalues λ_i have been calculated for three flow cases with different Ar . Comparing these coherent structures with the structure of time averaged velocity maps and analysing the eigenvalues it is found that with increasing Ar an increase of the number of energy eigenvalues exceeding the noise level can be observed. Particularly, in the case dominated by forced convection (regime of $Ar = 0.89$) only one eigenvalue exceeds the noise level. In addition it can be remarked that the eigenvalues of the mode mainly related to the inertia-induced motion decrease from 86 % to 35 % of the total energy in the regime $Ar = 0.89 - 1.6$. This is in contrast to the buoyancy-induced motion related mode which increases. While at $Ar = 0.89$ the influence of buoyancy-induced motion is negligible the eigenvalue of this mode increases to 24 %

of the total energy for $Ar = 1.6$. Further due to the increasing buoyancy force the flow structure of the time averaged velocity map changes from a nearly two dimensional role structure to a bimodal structure which has been found for $Ar = 1.6$.

Additionally the spectra of the time coefficient $\zeta_i(t)$ and the outlet temperature time series were shown. Comparing the spectra for the cases $Ar = 1.24$ and $Ar = 1.6$ concurrent resonance frequencies for several modes have been observed.

7 References

- [1] Linden PF. The fluid mechanics of natural ventilation. *Annu. Rev. Fluid Mech.*, Vol. 31, pp 201-238, 1999.
- [2] Linden PF, Lane-Serff GF and Smeed DA. Emptying filling boxes the fluid mechanics of natural ventilation. *J. Fluid Mech.*, Vol. 212, pp 300-335, 1990.
- [3] Hunt GR and Linden PF. The fluid mechanics of natural ventilation - displacement ventilation by buoyancy-driven flows assisted by wind. *Proc. ROOMVENT, 5th Int. Conf. on Air Distrib. in Rooms*, vol. 3, pp 239-46, 1996.
- [4] Fleischer AS and Goldstein RJ. High-Rayleigh-number convection of pressurized gases in a horizontal enclosure. *J. Fluid. Mech.*, vol. 469, pp 1-12, 2002.
- [5] Niemela JJ, Skrebek L and Donnelly RJ. Turbulent convection at very high Rayleigh numbers. *Nature*, vol. 404, pp 837-840, 2000.
- [6] Chiu KC, Ouazzani J and Rosenberger F. Mixed convection between horizontal plates - I. Entrance effects. *Int. J. Heat Mass Transfer*, vol. 30, pp.1648:1654, 1987.
- [7] Chiu KC, Ouazzani J and Rosenberger F. Mixed convection between horizontal plates - II. Fully developed flow. *Int. J. Heat Mass Transfer*, vol. 30, pp.1655:1662, 1987.
- [8] Smits AJ and Zagarola MV. Applications of dense gases to model testing for aeronautical and hydrodynamic applications. *Meas. Sci. Technol.*, vol. 16, 1710:1715, 2005
- [9] Willert C and Jarius M. Planar flow field measurements in atmospheric and pressurized combustion chambers. *Exp. in Fluids*, vol. 33, pp. 931:939, 2002.
- [10] Sirovich L. Turbulence and dynamics of coherent structures. Part I: Coherent structures. *Quart. of App. Math.*, no. 3, pp. 561-571, 1987.
- [11] Sirovich L. Turbulence and dynamics of coherent structures. Part II: Symmetries and transformations. *Quart. of App. Math.*, no. 3, pp. 573-582, 1987
- [12] K. Xia, C. Sun and S. Zhou. Particle image Velocimetry measurement of velocity field in turbulent thermal convection. *Physical review E*, no. 68-066303, 2003
- [13] Bosbach J, Kühn M, Wagner C, Raffel M, Resagk C, du Puits R and Thess A. Large-scale particle image velocimetry of natural and mixed convection. *13th Int. Symp. on Applications of Laser Techniques to Fluid Mechanics*, 2006.
- [14] Silekens JJM, Rindt CCM and Van Steenhoven AA. Developing Mixed Convection in a Coiled Heat Exchanger. *Int. Journal of Heat and Mass Transfer*, vol. 41, pp 61-72, 1998.
- [15] Westhoff A, Grabinski N, Bosbach J, Wagner C. and Thess A. Scaling of Turbulent Mixed Convection under High Pressure. *5th Int. Symposium on Turbulence and Shear Flow Phenomena*, vol. 3, pp 505-512, 2007.
- [16] Westhoff A, Grabinski N, Bosbach J, Wagner C. and Thess A. Particle Image Velocimetry of Turbulent Mixed Convection at Ambient and High Pressure. *8th Int. Symposium on Experimental and Computational Aerothermodynamics of Internal Flows*, vol. 2, pp 281-290, 2007.

The authors confirm that they, and/or their company or institution, hold copyright on all of the original material included in their paper. They also confirm they have obtained permission, from the copyright holder of any third party material included in their paper, to publish it as part of their paper. The authors grant full permission for the publication and distribution of their paper as part of the ICAS2008 proceedings or as individual off-prints from the proceedings.